Preprints of the 21st IFAC World Congress (Virtual)
Berlin, Germany, July 12-17, 2020

Intersection-Traffic Control of Autonomous Vehicles using Newton-Raphson Flows and Barrier Functions

S. Shivam [*], **Y. Wardi** [*], **M. Egerstedt** [*], **A. Kanellopoulos** [**], **K. G. Vamvoudakis** [**]

[*] *School of Electrical and Computer Engineering, Georgia Institute of Technology, Atlanta, GA 30332, USA.*
e-mail: sshivam6@gatech.edu, ywardi@ece.gatech.edu, magnus@ece.gatech.edu.
[**] *The Daniel Guggenheim School of Aerospace Engineering, Georgia Institute of Technology, Atlanta, GA,* 30332*, USA.*
e-mail: ariskan@gatech.edu, kyriakos@gatech.edu.

Abstract: This paper concerns an application of a recently-developed nonlinear tracking technique to trajectory control of autonomous vehicles at traffic intersections. The technique uses a flow version of the Newton-Raphson method for controlling a predicted system-output to a future reference target. Its implementations are based on numerical solutions of ordinary differential equations, and it does not specify any particular method for computing its future reference trajectories. Consequently it can use relatively simple algorithms on crude models for computing the target trajectories, and more-accurate models and algorithms for trajectory control in the tight loop. We demonstrate this point on an extant predictive traffic planning-and-control method with our tracking technique. Furthermore, we guarantee safety specifications by applying to the tracking technique the framework of control barrier functions.

1. INTRODUCTION

In a recent work (Wardi et al. (2019)), we proposed a new approach to output tracking of dynamical systems that appears to be effective while requiring modest computing efforts. Its underscoring technique is based on a standalone integrator with a variable gain, designed for stability and small tracking errors. The integrator is defined by a flow version of the Newton-Raphson method for solving algebraic equations. These equations are defined by attempting to match a predicted system's output to a predicted value of the reference target. Furthermore, increasing the controller's rate can stabilize the system, increase its stability margins, and reduce its tracking error even (in some cases) if the plant-subsystem is unstable and not of a minimum phase.

Formally, consider the system depicted in Figure 1, where the reference input $r(t)$, the control signal $u(t)$, and the output $y(t)$ are in R^m for a given $m = 1, 2, \ldots$. Suppose that the plant is a dynamical system with the state equation

$$\dot{x}(t) = f(x(t), u(t)),\ x(0) := x_0, \tag{1}$$

and the output equation

$$y(t) = h(x(t)); \tag{2}$$

⋆ This work was supported in part by the National Science Foundation under grant Nos. S&AS-1849264, CPS-1851588, and by ONR Minverva under grant No. N00014-18-1-2874.

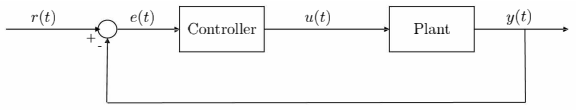

Fig. 1. Basic control system.

here the state variable is $x(t) \in R^n$, $x_0 := x(0) \in R^n$ is a given initial state, and the dynamic-response function $f : R^n \times R^m \to R^n$ and output function $h : R^n \to R^m$ satisfy the following assumption:

Assumption 1. 1). The function $f : R^n \times R^m \to R^n$ is continuously differentiable, and for every compact set $\Gamma \subset R^m$ there exists $K > 0$ such that, for every $x \in R^n$ and for every $u \in \Gamma$,

$$\|f(x, u)\| \leq K\big(\|x\| + 1\big). \tag{3}$$

2). The function $h : R^n \to R^m$ is continuously differentiable.

This assumption guarantees a unique continuous, piecewise-continuously differentiable solution $x(t)$ to Eq. (1) for every bounded, piecewise-continuous input $u(t)$ and an initial condition x_0.

The controller is defined as follows. Fix $T > 0$. At time $t \geq 0$, let $\hat{y}(t + T)$ be a predicted value of $y(t + T)$, which is assumed to depend on $x(t)$ and $u(t)$. We denote this dependence by the functional notation

$$\hat{y}(t + T) = g(x(t), u(t)), \tag{4}$$

and assume that the function $g : R^n \times R^m \to R^m$ is continuously differentiable. The output predictor that we use is based on simulating the system, at time t, over the time-interval $[t, t+T]$, with the initial condition $x(t)$ and the constant input $u(\tau) := u(t)$ for all $\tau \in [t, t+T]$. Thus, we numerically solve the equation

$$\dot{\xi}(\tau) = f(x(\tau), u(t)), \qquad \xi(t) = x(t) \tag{5}$$

by the forward-Euler method, then we define

$$\hat{y}(t+T) := \xi(t+T). \tag{6}$$

We mention that the future reference $r(t+T)$ also may have to be estimated by a suitable predictor (e.g., Wardi et al. (2019)), but we assume here that it is known exactly at time t in order to simplify the discussion.

The controller is defined by the following equation,

$$\dot{u}(t) = \alpha\Big(\frac{\partial g}{\partial u}(x(t), u(t))\Big)^{-1}\big(r(t+T) - g(x(t), u(t))\big) \tag{7}$$

with given gain $\alpha > 0$ and initial condition $u_0 := u(0)$; we implicitly assume that the partial Jacobian $\frac{\partial g}{\partial u}(x(t), u(t))$ is nonsingular along the trajectory $(x(t), u(t))$ in the forthcoming discussion. The tracking convergence of this controller has been analyzed in Wardi et al. (2019), and the results are summarized in the expanded version of this paper published in the Arxiv (Shivam et al. (2020)).

Thus far, the development of the aforementioned tracking technique has focused on its fundamental structure, theoretical convergence results, and various examples including an inverted pendulum and motion control in platoons (Wardi et al. (2019)). Presently our main interest is in applications to autonomous vehicles, and especially in trajectory control of swarms and platoons. Such problems often are being addressed by Model Predictive Control (MPC) or related techniques; see e.g., (Kong et al. (2015); Plessen et al. (2018); Kim and Kumar (2014)) and references therein. Like MPC, our tracking technique is based on prediction, but it is different from MPC in the following ways. 1). It is not based on optimal control nor does it specify a particular framework for computing future target trajectories. 2). Its reliance on the Newton-Raphson flow gives it a fast convergence. 3). The prediction horizon may, but does not have to be short. 4). The predictor and controller, defined by Eqs. (5)–(7), can be implemented in real time by the forward Euler method.

The primary objective of this paper is to investigate how the proposed tracking framework can complement the prediction-based trajectory-control technique, developed in Malikopoulos et al. (2018) for traffic management of autonomous vehicles in urban road-intersections. This technique is slated to optimize motion-energy consumption of each vehicle while guaranteeing safety constraints. It is in the flavor of MPC in that it solves optimal control problems for computing future trajectories, but unlike MPC it does not consider rolling horizons but a single optimal control program for each vehicle approaching an intersection. A salient feature of this technique is that it uses a simple dynamic model for the vehicles, comprised of a double integrator, thereby enabling closed-form solutions to the optimal control problems. This gives an efficient trajectory-computation for every vehicle, which scales well with traffic loads at the intersections.

Our tracking technique complements the traffic control framework of Malikopoulos et al. (2018) in the following way. We first compute the target-trajectories of the vehicles using the simple model and formula derived in Malikopoulos et al. (2018), then we apply our technique to a more complicated and realistic model for tracking the computed trajectories. To this end we use a dynamic bicycle model for the vehicles' motion, a sixth-order nonlinear model that has been extensively used in the control of autonomous vehicles (see, e.g., Kong et al. (2015); Plessen et al. (2018) and references therein). Furthermore, we extend the applications domain of Malikopoulos et al. (2018) from a straight road to a curved road. Lastly, we examine the treatment of safety constraints in the tight control loop by incorporating control barrier functions with the tracking technique.

The rest of the paper is organized as follows. Section 2 formulates the problem, Section 3 presents simulation results, and Section 4 concludes the paper and outlines directions for future research.

Statement of contributions. The contribution of the present paper is twofold: Extending the framework of prediction-based tracking in the context of trajectory control of autonomous vehicles, and incorporating safety measures through the use of barrier functions. The tracking technique has been applied to the dynamic bicycle model (Shivam et al. (2019); Wardi et al. (2019)), and the relevant contribution in this paper is in its application to the control framework of Malikopoulos et al. (2018). Regarding safety guarantees, control barrier functions have not been applied to the tracking technique or, to our knowledge, to a dynamic bicycle model.

2. PROBLEM FORMULATION

Our work is concerned with the management and control of vehicle-flows at traffic intersections. Following Malikopoulos et al. (2018), each one of the roads comprising an intersection consists of two zones: a control zone and a merging zone. The merging zone is at the center of the intersection, where lateral accidents are possible. The control zone is a stretch of the road approaching the merging zone, where the scheduling, planning and control of vehicles' trajectories are performed. Once a vehicle enters the merging zone its speed or lane cannot be changed.

Whenever a vehicle enters the control zone, a scheduler computes the time and speed at which it has to enter the merging zone based on the current and future states (positions and velocities) of all the other vehicles concurrently in the intersection. Subsequently the trajectory of the newly-arrived vehicle is computed by minimizing its projected motion energy while maximizing the throughput at the intersection, subject to safety and operational constraints. The safety constraints include a minimum inter-vehicle distance and a maximum deviation from a lane-center, while the operational constraints include bounds on speed and acceleration. This trajectory-planning problem is formulated as an optimal control problem which is parameterized by the states of all the other vehicles concurrently at the intersection, hence it is different from one vehicle to the next and consequently must be solved in real time.

The contribution of this paper is not in the aforementioned scheduling and trajectory planning-and-control problem, but in a tracking of its computed solution. Thus, the tracking control is at a lower level than the optimal control problem, and for that we use a bicycle model for the vehicles' dynamics, which is more accurate and detailed than the double-integrator model.

The bicycle model that we use is the six-degree nonlinear system described in Kong et al. (2015). Its state variable is $x = (z_1, z_2, v_\ell, v_n, \psi, \dot{\psi})^\top$, where z_1 and z_2 are the planer position-coordinates of the center of gravity of the vehicle, v_ℓ and v_n are the longitudinal and lateral velocities, ψ is the heading of the vehicle and $\dot{\psi}$ is its angular velocity. The input, $u = (a_\ell, \delta_f)^\top$, consists of the longitudinal acceleration and steering angle of the front wheels, respectively, and the output, $y = (z_1, z_2)^\top$, is the center of gravity of the vehicle. The dynamic equations are (see Kong et al. (2015)):

$$\begin{aligned}
\dot{z}_1 &= v_\ell \cos\psi - v_n \sin\psi, \\
\dot{z}_2 &= v_\ell \sin\psi + v_n \cos\psi, \\
\dot{v}_\ell &= \dot{\psi} v_n + a_\ell, \\
\dot{v}_n &= -\dot{\psi} v_\ell + 2\left(F_{c,f}\cos\delta_f + F_{c,r}\right)/m, \\
\ddot{\psi} &= 2\left(l_f F_{c,f}\cos\delta_f - l_r F_{c,r}\right)/I_z,
\end{aligned} \tag{8}$$

where m is the mass of the vehicle, l_f and l_r are the front and back axles' distances from the vehicle's center of mass, I_z is the yaw moment of inertia, and $F_{c,f}$ and $F_{c,r}$ are the lateral forces on the front and rear tyres. These forces are approximated by the following equations,

$$\begin{aligned}
F_{c,f} &= C_{\alpha,f}\left(\delta_f - \tan^{-1}\left((v_n + l_f\dot{\psi})/v_\ell\right)\right), \\
F_{c,r} &= -C_{\alpha,r}\tan^{-1}\left((v_n - l_r\dot{\psi})/v_\ell\right),
\end{aligned}$$

where $C_{\alpha,f}$ and $C_{\alpha,r}$ are the cornering stiffness of the front and rear tyres, respectively.

Our tracking technique will be tested first on a curved road, which does not quite fit in the framework of Malikopoulos et al. (2018) due to its one-dimensional traffic model of motion. Then we make a more careful examination of safety constraints which are addressed in real time by control barrier functions, and for that we use a straight road in order to highlight the effects of the safety controls.

3. SIMULATION RESULTS

We consider the control zone of a road approaching an intersection, and as in Malikopoulos et al. (2018), assume that vehicles do not change lanes and hence we focus on a single lane. The motion dynamics of the vehicles follow the bicycle model discussed in Section 2 with the following parameter values as in Shivam et al. (2019): $m = 2,050\ kg$, $I_z = 3,344\ kg \cdot m^2$, $l_f = 1.105\ m$, $l_r = 1.738\ m$, $C_{\alpha,f} = 57500\ N/rad$, and $C_{\alpha,r} = 92500\ N/rad$.

Two experiments are conducted. In the first experiment we consider only tracking without regard to safety constraints in the tight loop. We compute the trajectories of the vehicles by the formula derived in Malikopoulos et al. (2018), then apply the tracking technique to ensure that the computed trajectories are followed. In the second experiment we define safety constraints in terms of minimum inter-vehicle distance and maximum lateral deviations from the lane's center, and apply control barrier functions to ensure that they are satisfied in the face of unexpected changes to traffic conditions.

3.1 Tracking Control

We consider a road (lane) approaching an intersection, consisting of 400m control zone and 30m merging zone, and comprising a 30^o arc of a circle with a radius of 821.23m. There are 5 vehicles in the experiment. They arrive to the control zone at randomly-drawn times, all at the same initial speed of 13.4 m/s and longitudinal acceleration of 0. The initial heading of all the vehicles is 0^o with respect to the direction of the lane, and therefore, if the control gives effective tracking, they are expected to remain close to the lane's center and maintain a heading of near 0^o (with respect to the road) throughout the control zone.

The arrival times of the vehicles to the merging zone and the vehicle's trajectories in the control zone are computed, respectively, by the scheduling procedure and the optimal control algorithm proposed in Malikopoulos et al. (2018). Now it must be pointed out that that algorithm is applicable to straight roads since it is underscored by a straight-line model of motion. Therefore, we compute the trajectories as if the road is straight, and map the results to the curved road according to the distance travelled.

To test the robustness of the controller with respect to modeling variations, we induce an error of 100% in the vehicles' mass. Thus, the predictor equation (4) uses twice the "real" weight of the cars which is used in the simulations.

All the differential equations for the simulation and the controller are solved by the Forward Euler method with step-size of $\mathrm{d}t = 0.005$ for the simulations, and $\Delta t = 0.001$ for the controller. The controller speedup factor is set at $\alpha = 100$.

The results are shown in Figures 2-4. Figure 2 depicts the graphs of the distance (arc-length) travelled by the five vehicles through the control zone and merging zone, as functions of time. The color-coded legend indicates the order of the vehicles according to their arrivals to the control zone. The vehicles' distance-travelled graphs are extended beyond their departures from the intersection at the constant of 430m for the sake of a better presentation. Apparently Car 1 moves at a constant velocity. In contrast, subsequent vehicles slow down in order to meet the computed schedule of entering the merging zone, which is more sparse than their arrival schedule to the control zone.

The tracking error for each vehicle, defined by the Euclidean distances between its position and target reference as computed by the optimal control program, is depicted in Figure 3. Following an initial error of about 6 cm, the vehicles settle, in about 3 seconds, to a steady-state error of under 2 cm. The initial error is due to transients associated with discrepancies between the vehicles' initial poise and their corresponding reference points. These transients appear identical for all the vehicles, because their respective initial positions, velocities and steering angles are identical

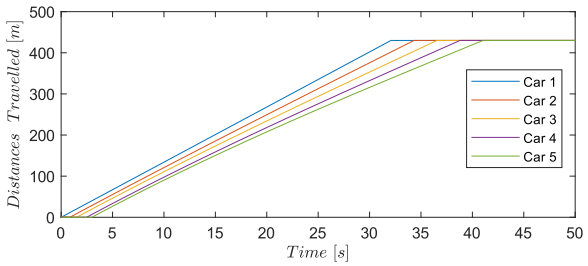

Fig. 2. Distances traveled vs. time, barely distinguishable from the corresponding target trajectories.

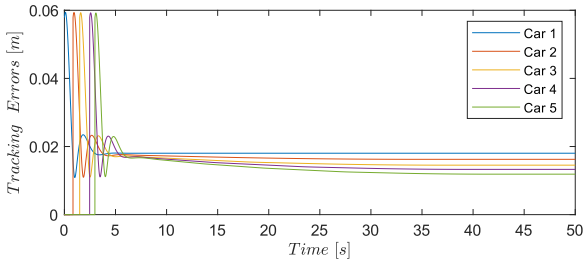

Fig. 3. Tracking errors vs. time, under 6 cm during initial transient phase, and under 2 cm thereafter.

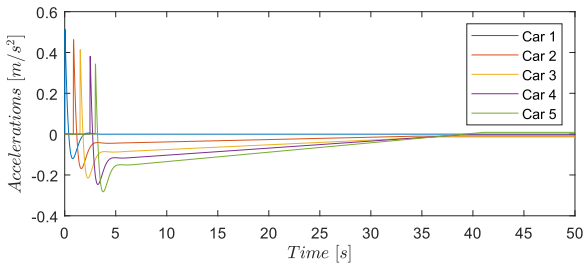

Fig. 4. Vehicles' longitudinal accelerations vs. time, under 5% of g.

when they enter the control zone. The asymptotic tracking errors are due to the prediction errors and the curvatures of the road; a test of this hypothesis by simulations is described in Shivam et al. (2020). Since the tracking errors are small relative to the distance travelled, the graphs in Figure 2 are indistinguishable from corresponding graphs of the reference trajectories, which consequently are not presented in the paper.

Figure 4 depicts the graphs of the longitudinal accelerations of the vehicles vs. time, and we observe initial transients of under 0.48 m/s^2. The graphs of later vehicles are below the graphs of earlier vehicles. This is due to the fact that all of the vehicles travel the same distance but later ones do it in more time, hence have to decelerate more than earlier vehicles. We also note that each graph reaches zero acceleration at the final point of the control zone, which is in compliance with the constraint that it must travel across the merging zone at a constant speed.

3.2 Incorporation of Safety Constraints

We next extend the simulation setting described in the last subsection to include safety constraints that are addressed by Control Barrier Functions (CBF). Refs. Ames et al. (2014, 2017) laid the groundwork for a CBF framework which guarantees safety in the tight-loop control. The framework combines control barrier functions with control Lyapunov functions to achieve the dual purpose of effective control while satisfying hard safety constraints. Shortly thereafter it was applied to the control of multi-agent systems and networks, with applications to mobile robots and autonomous vehicles; see Wang et al. (2017) for an initial work, and Ames et al. (2019) for a recent survey. The gist of the CBF approach is to compute a control signal based on a feedback law, then project it into a set in the input space which guarantees safety. If the plant-dynamics are control affine, the projection comprises the solution of a quadratic program which may be computable in real time. A brief summary of CBF in the context of the problem described in this paper can be found in Shivam et al. (2020).

To highlight the salient features of the CBF approach, we henceforth consider only two vehicles travelling on a straight, single-lane road. The first vehicle serves as an obstacle for the second vehicle, hence its trajectory is predetermined and not controlled. The second vehicle has the same dynamic bicycle model as in Subsection 3.1, and it is controlled by the same tracking technique described there.

The first vehicle enters the control zone at time $t = -5$ s, and the second vehicle enters it at time $t_0 := 0$. The first vehicle travels along the road and its speed profile is shown in the blue graph of Figure 5. The piecewise-constant velocities in the figure are 2 m/s, 1 m/s, and 2 m/s, respectively; its deceleration commences at time t_1:=50 s, and its acceleration starts at time t_2:=75 s. It travels along the lane without lateral deviations.

At the time the second vehicle enters the control zone (road), $t_0 = 0$, it is 10m behind the first vehicle. Its target reference trajectory is $r_2(t) := r(t) = (2t, 0)^\top$, lying along the road. However, it enters the road at the initial steering angle of 20^o, or 0.35 rad from the direction of the road. Therefore initially the second vehicle veers off the lane, but is pulled back to it by the tracking control. Thereafter it stays on the lane while attempting to track its target trajectory. Without an application of the CBF to the second vehicle, maximum deviation (lateral distance) from the lane's center is about 1.6m, which practically may be unacceptable. Furthermore, after returning to the lane, it runs into the first vehicle shortly after its slowdown.

To avoid the collision and limit the lateral deviation from the lane, we impose the following two safety constraints: (i) the second vehicle must maintain a distance of at least 5m from the first vehicle, and (ii) the lateral deviation of the second vehicle from the center-lane must not exceed 0.5m. We label these the *longitudinal constraint* and the *lateral constraint*. We design two corresponding CBF and apply them jointly with the tracking controller. We point out that the longitudinal dynamics of the second vehicle are control-affine while its lateral dynamics are not control affine; see the state equation (8).[1] Therefore the CFB projection for the longitudinal constraint can be computed by a quadratic program while the lateral CBF projection

[1] We are aware of a transformation of the system that renders its state equation affine with respect to both input controls (Rajamani (2012)). However, we prefer to work with the current system in order to test the controller in an environment where the state equation is not control affine.

has to rely on an alternative, ad-hoc algorithm. We next explain the two control barrier functions.

Let us denote the position and velocity of the ith vehicle, $i = 1, 2$, by $p_i \in R^2$ and $v_i \in R^2$, respectively. Furthermore, define the relative displacement and relative velocity of the second vehicle with respect to the first one by $\Delta p := p_1 - p_2$ and $\Delta v := v_1 - v_2$. The purpose of the CBF is to ensure that $||\Delta p|| \geq d_0$ for a given $d_0 > 0$ ($d_0 = 5$m in our experiments). Therefore it is tempting to define the safe set as $\mathcal{S} := \{x \in R^6 \ : \ ||\Delta p|| \geq d_0\}$, where x is the state variable of the dynamic bicycle model defined by Eq. (8). However, this does not guarantee that collisions cannot occur due to the inertia inherent in the dynamic model.

To get around this difficulty we use an idea, developed in Wang (2018), of defining a CBF in terms of the relative velocity along the relative displacement. Denoted by $\hat{v}$, it is defined by

$$\hat{v} = \langle \frac{\Delta p}{\|\Delta p\|}, \Delta v \rangle. \tag{9}$$

Let $\bar{a} > 0$ denote the maximum-possible longitudinal deceleration of the second vehicle, and define $k := (2\bar{a})^{-1}$. Recall that the longitudinal acceleration is denoted by a_ℓ and it is a part of the input (see (8)). Now, a simple algebra shows that for every interval $[t, t_1]$ where the first vehicle has a constant velocity, if $a_\ell(\tau) \equiv -\bar{a}$ then $||\Delta p(\tau)|| \geq ||\Delta p(t)|| - k\hat{v}(t)^2$. Therefore, to ensure the forward invariance of the constraint set $\{x \in R^6 : \|\Delta p\| \geq d_0\}$, we impose the condition that

$$\|\Delta p(t)\| - k\hat{v}(t)^2 \geq d_0. \tag{10}$$

This leads us to define the barrier function by $h(x) = \sqrt{k(\|\Delta p\| - d_0)} - ||\hat{v}||$. As a part of the safety control we enforce the condition $\frac{d}{dt}h(x(t)) + h(x(t)) \geq 0 \ \forall t \geq 0$, which implies that the set defined by (10) is forward invariant (see Ames et al. (2014, 2017, 2019)). Therefore, we consider the set defined by (10) as the safe set. Finally, we note that the dynamic equation (8) is control affine in the longitudinal acceleration, and hence the input control can be computed by a quadratic program.

To define the lateral CBF, we only need the lateral deviation of the vehicle from the lane's center and its velocity. Denote by y the lateral deviation, and let $y_{\max}$ be the maximum allowed deviation. In analogy with (10), the following condition ensures the maximum deviation constraint,

$$y_{\max} \geq \left| y + k\frac{y}{|y|}\dot{y}^2 \right|, \tag{11}$$

where $k := (2\tilde{a})^{-1}$ with $\tilde{a}$ denoting the maximum lateral acceleration. We define the safe set to be the set satisfying the inequality in (11), and correspondingly, we define the barrier function $h(x) := y_{\max} - |y + k\frac{y}{|y|}\dot{y}^2|$. Further defining (after some trial and error) $\kappa(h) = 15h^3$, it can be seen that $\frac{d}{dt}h(x(t)) = \kappa(h(x)) \geq \forall t \geq 0$ thereby ensuring safety (see Ames et al. (2014, 2017, 2019)).

The input involved with the lateral deviation is the steering angle of the front wheels, δ_f. Since the state equation is not control-affine in this input, its projection into the safe set cannot be computed by a quadratic program. Instead, we compute the projection by a bisection line search over the allowable input set which is the interval $[-\frac{\pi}{4}, \frac{\pi}{4}]$.

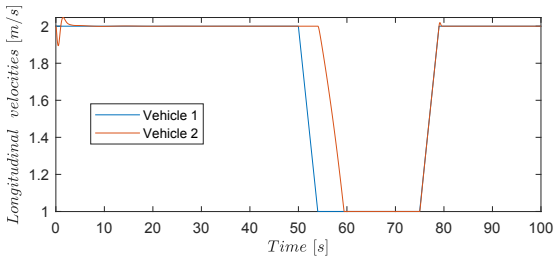

Fig. 5. Vehicles' velocities vs. time. The change in velocity of Car 2 is due to the action of the CBF.

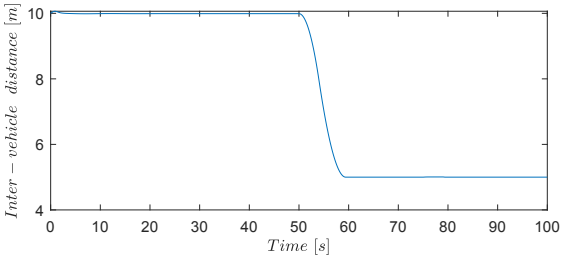

Fig. 6. Distance between the two vehicles. The decline starting at 50s is due to the action of the CBF.

The simulation results are shown in Figures 5-10. Figure 5 depicts the speeds of the first and second vehicles in blue and red, respectively. The visible initial transient of the red graph is due to the heading of the car when it enters the road. Note the delay in the slowdown of the second vehicle after the first vehicle; it is due to the fact that the second vehicle starts reducing its speed not immediately but when its distance from the first vehicle approaches the minimum of 5 m. In contrast, there is no such delay in the speedup since that would violate the minimum-distance constraints. Figure 6 shows the graph of the inter-vehicle distance, and we clearly see that it retains its minimum value through and following the speedup of the first vehicle.

Figure 7 depicts the graph of the lateral (normal) deviation of the second vehicle from the lane's center, which is largely due to its initial heading of 20^o. We mentioned that without the lateral CBF the maximum distance is 1.6 m, and we observe that with the CBF, the maximum distance is about 0.27 m. Figure 8 shows the graph of the distance between the position of the second vehicle and its target trajectory. Following an initial transient the vehicle catches up and tracks its target trajectory until the first vehicle slows down. It then rises during the slowdown period due to the action of the CBF. After the first vehicle speeds up, the second vehicle cannot close down its tracking error since it is forced by the CBF to keep the inter-vehicle distance of 5 m, hence the tracking error assumes a constant value.

The next two figures show the two controls. Figure 9 depicts the longitudinal acceleration, and we notice jumps that are due to initial transients as well as the slowdown and speedup of the first-vehicle. Figure 10 depicts the graph of the steering angle of the second car, and it displays a transient due to the initial heading of the car. Neither figure displays surprising results.

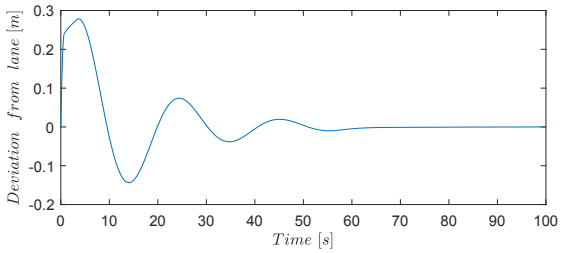

Fig. 7. Distance of second vehicle from the lane-center. Without the CBF the maximum distance is about 1.6m.

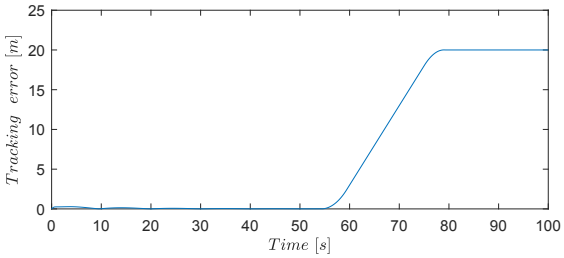

Fig. 8. Tracking error of second vehicle. It cannot be reduced due to the CBF.

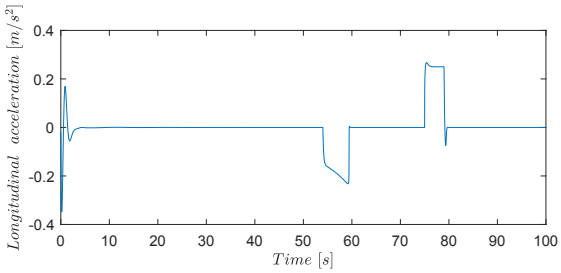

Fig. 9. Longitudinal acceleration of second vehicle.

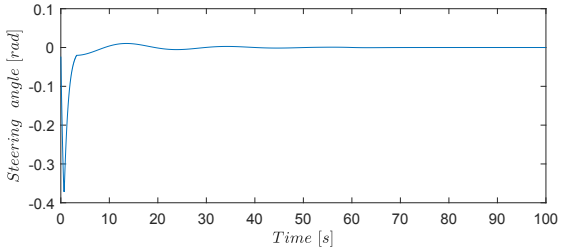

Fig. 10. Steering angle of second vehicle

4. CONCLUSION AND FUTURE WORK

This work applies a specific prediction-based, nonlinear tracking technique to the trajectory control of autonomous vehicles at traffic intersections. We guarantee safety specifications by applying to the tracking technique the framework of control barrier functions. Future work will focus on developing robustness guarantees that will allow for more realistic scenarios, where modeling inaccuracies and external disturbances are taken into consideration.

REFERENCES

Ames, A., Coogan, S., Egerstedt, M., Notomista, G., Sreenath, K., and Tabuada, P. (2019). Control barrier functions: Theory and applications. In *European Control Conference,* Napoli, Italy, June 25-28.

Ames, A., Grizzle, J., and Tabuada, P. (2014). Control barrier function based quadratic programs with application to adaptive cruise control. In *IEEE Conf. Decision and Control (CDC),* Los Angeles, California, December 15-17, 6271–6278.

Ames, A., Xu, X., Grizzle, J., and Tabuada, P. (2017). Control barrier function based quadratic programs for safety critical systems. *IEEE Trans. Automatic Control*, 62, 3861–3876.

Kim, K.D. and Kumar, P. (2014). Am mpc-based approach to provable system-wide safety and liveness of autonomous ground traffic. *IEEE Transactions on Automatic Control*, 59(12), 3341–3356.

Kong, J., Pfeiffer, M., Schildbach, G., and Borrelli, F. (2015). Kinematic and dynamic vehicle models for autonomous driving control design. In *Proc. IEEE Intelligent Vehicles Symposium (IV)*.

Malikopoulos, A., Cassandras, C., and Zhang, Y. (2018). A decentralized energy-optimal control framework for connected automated vehicles at signal-free intersections. *Automatica*, 93, 244–256.

Plessen, M., Bernardini, D., Esen, H., and Bemporad, A. (2018). Spatial-based predictive control and geometric corridor planning for adaptive cruise control coupled with obstacle avoidance. *IEEE Transactions on Control Systems Technology*, 26(4), 38–50.

Rajamani, R. (2012). *Vehicle Dynamics and Control*. Springer, New York, New York.

Shivam, S., Buckley, I., Wardi, Y., Seatzu, C., and Egerstedt, M. (2019). Tracking control by the Newton-Raphson flow: Applications to autonomous vehicles. In *2019 European Control Conference (ECC 2019),* Napoli, Italy, June 25-28.

Shivam, S., Wardi, Y., Egerstedt, M., Kanellopoulos, A., and Vamvoudakis, K. (2020). Intersection-traffic control of autonomous vehicles using newton-raphson flows and barrier functions. In *arxiv,* http://arxiv.org/abs/*2004.10226*.

Wang, L., Ames, A., and Egerstedt, M. (2017). Safety barrier certificates for collisions-free multi-robot systems. *IEEE Transactions on Robotics*, 33(3), 661–674.

Wang, L. (2018). *Multi-Robot Coordination and Safe Learning Using Barrier Certificates*. Ph.D. thesis, Georgia Institute of Technology.

Wardi, Y., Seatzu, C., Cortes, J., Egerestedt, M., Shivam, S., and Buckley, I. (2019). Tracking control by the newton-raphson method with output prediction and controller speedup. In *arxiv,* http://arxiv.org/abs/1910.00693, submitted to *Automatica*.